Low Density Ionized Gas in the Inner Galaxy—Interpretation of Recombination Line Observations at 325 MHz

K. R. Anantharamaiah *Raman Research Institute, Bangalore 560080*

Abstract. The recent survey of H 272α recombination line (324.99 MHz) in the direction of 34 Hɪɪ regions, 12 SNRs and 6 regions of continuum minimum ('blank' regions) in the galactic plane is used to derive the properties of diffuse ionized gas in the inner Galaxy.

The intensity of radio recombination lines at high frequencies is dominated by spontaneous emission in high-density gas and that at low frequencies (325 MHz) by stimulated emission in low-density gas. We have used this property to obtain the electron density in the gas in the direction of blank regions and SNRs, by combining the H 272α measurements (preceeding paper) with the published data at higher frequencies. Further, we have imposed constraints on the electron temperature and pathlength through this gas using the observed high-frequency continuum emission, average interstellar electron density and geometry of the line-emitting regions. The derived properties of the gas are (i) electron density 0.5–6 cm^{-3}, (ii) electron temperature 3000–8000 K and (iii) emission measures 500–3000 pc cm^{-6}. The corresponding pathlengths are 50–200 pc.

As the derived sizes of the low-density regions are small compared to the pathlength through the Galaxy, the low-frequency recombination lines cannot be considered as coming from a widely distributed component of the interstellar medium.

The Hɪɪ regions studied in the above survey cannot themselves produce the H 272α lines detected towards them because of pressure broadening, optical depth, and beam dilution. However, the agreement in velocity of these lines with those seen at higher frequencies suggests that the low-frequency recombination lines arise in low-density envelopes of the Hɪɪ regions. Assuming that the temperature of the envelopes are similar to those of the cores and invoking geometrical considerations we find that these envelopes should have electron densities in the range 1–10 cm^{-3} and linear sizes of 30–300 pc in order to produce the observed H 272α lines.

Key words: Galaxy, recombination lines—galactic ridge—interstellar medium, electron densities—Hɪɪ regions, low density envelopes

1. Introduction

Recombination lines observed at low frequencies (< 1 GHz) preferentially sample conditions in low-density regions whereas those at higher frequencies originate mainly

in higher-density regions. Several surveys of recombination line emission from the galactic plane have been performed at high frequencies (> 1 GHz) (see Wilson 1980 and references therein), and have been used for deducing the properties of the ionized regions. Until recently, recombination line observations at low frequencies (and therefore from correspondingly lower-density regions) were available towards only a few sources in the galactic plane (see Pedlar & Davies 1980 and references therein). Some of these observations have been used to deduce the properties of low-density regions (*e.g.* Shaver 1976) and to demonstrate the importance of stimulated emission of recombination lines at low frequencies (Pedlar *et al.* 1978).

Apart from the discrete ionized regions (HII regions) in the galactic plane there is evidence for the presence of more widespread lower-density ionized gas in the inner Galaxy from what are known as 'galactic ridge recombination lines' (Gottesman & Gordon 1970; Jackson & Kerr 1975; Lockman 1976; Hart & Pedlar 1976b, and see Lockman 1980 and references therein). These lines which have been observed mainly at centimetre wavelengths are seen in directions in the galactic plane apparently free of discrete continuum sources. There were no low-frequency observations of the ridge lines.

Recently, a survey was made of the recombination line emission at 325 MHz towards 53 directions in the galactic plane consisting of 34 HII regions, 12 SNRs and 6 'blank' regions which are free of discrete continuum sources (Anantharamaiah 1985a, hereafter referred to as Paper I). In Paper I we have presented the observations and the parameters of the H 272α lines detected towards 47 of these directions. A discussion of the broad characteristics of the data was also presented in Paper I and it was shown that most of the observed lines arise due to stimulated emission in the presence of background radiation. In this paper we make use of the observed parameters and derive the physical properties of the ionized regions responsible for these lines. In Section 2 we present some general considerations and a brief summary of the relevant theory of line formation. In Section 3 we obtain the properties of the ionized gas observed towards blank regions and SNRs, and in Section 4 towards HII regions. A discussion of the derived parameters is presented in the final section.

2. General considerations

The detection of a recombination line in a given direction essentially yields three line parameters, the peak line intensity T_L, the full line width at half maximum intensity ΔV and the line centre velocity V_{LSR}. In addition, the average continuum beam brightness temperature T_{BC} is also measured in the same direction. V_{LSR} can indicate the distance to the source if a model of galactic rotation is used. As the total continuum temperature T_{BC} is dominated by the nonthermal galactic background, at this frequency, it is not possible to use the ratio of line to continuum temperature to derive the electron temperature of the region as usually done at higher frequencies. Further, even the thermal part of the continuum is dominated by emission from high-density ionized regions whereas the low-frequency recombination lines arise mostly in low-density regions (Brown *et al.* 1978). Therefore, at this frequency only the line intensity T_L and the width ΔV are directly related to the source parameters. However the total continuum temperature T_{BC} is an important quantity since it directly affects the line intensity T_L because of stimulated emission (Paper 1).

To derive or put constraints on the properties of the gas responsible for the observed lines, it is thus necessary to combine the line parameters from Paper I with other observations pertaining to the same gas.

2.1 *Theoretical Line Intensities*

Theoretical intensities of low-frequency recombination lines have been discussed in detail by Shaver (1975). The excess temperature produced at the recombination line frequency v by a homogeneous ionized region located in front of a background continuum source is given by

$$T_L = T_0 \left[e^{-\tau_C} (e^{-\tau_L} - 1) \right]$$
$$+ T_e \left[\frac{b_m \tau_L^* + \tau_C}{\tau_L + \tau_C} (1 - e^{-(\tau_L + \tau_C)}) - (1 - e^{-\tau_C}) \right]$$
$$+ T_N \left[\frac{1 - e^{-(\tau_L + \tau_C)}}{\tau_L + \tau_C} - \frac{1 - e^{-\tau_C}}{\tau_C} \right] \qquad (1)$$

where T_0 is the continuum temperature of the background source, T_e the electron temperature of the ionized region and T_N represents the nonthermal background distributed inside this region. The continuum optical depth is given by (Oster 1961)

$$\tau_C = 0.0314 \times v^{-2} T_e^{-3/2} \ln \left(4.955 \times 10^{-2} \frac{T_e^{3/2}}{v} \right) N_e N_i L \qquad (2)$$

where N_e and N_i (cm^{-3}) are the electron and ion densities, L (pc) is the pathlength through the region and v (GHz) is the frequency. In local thermodynamic equilibrium (LTE), the optical depth at the line centre (for α-lines) is given by (Shaver 1975)

$$\tau_L^* = \frac{8.796 \times 10^{-5} n^3}{\Delta V T_e^{5/2}} \left(1 + \frac{1.5}{n} \right) \exp \left(\frac{157890}{n^2 T_e} \right) (1 + 1.48\gamma)^{-1} N_e N_{H^+} L \qquad (3)$$

where n is the principal quantum number, N_{H^+} (cm^{-3}) is the ionized-hydrogen density, ΔV (km s^{-1}) is the full Doppler profile width at half maximum and γ is the ratio of the profile width due to pressure or radiation broadening to that due to pure Doppler broadening. The true optical depth in the line becomes

$$\tau_L = b_n \beta_n \tau_L^* \qquad (4)$$

with

$$\beta_n = 1 - \frac{k T_e}{hv} \frac{b_{n+1} - b_n}{b_n} \qquad (5)$$

where the departure coefficient b_n relates the true population, N_n of the atomic energy level n to its value in LTE, N_n^* by the equation

$$N_n = b_n N_n^*. \qquad (6)$$

The b_n values are usually calculated using the condition of time-independent statistical equilibrium which requires that there are as many transitions into a level as there are out of it (see for example Salem & Brocklehurst 1979). For calculations in this paper, we

have used the computer code published by Brocklehurst & Salem (1977) to obtain the b_n and β_n values.

2.2 *Upper Limit to the Electron Density from Observed Line Widths*

The width of a recombination line due to pressure broadening is directly proportional to the electron density in the region and is a strong function of the principal quantum number n (Griem 1967). The half-power width of the line due to this was calculated by Brocklehurst & Leeman (1971) under the impact approximation as

$$\Delta \nu_{LP} = 3.74 \times 10^{-11} \frac{N_e}{T_e^{0.1}} n^{4.4} \text{kHz}. \tag{7}$$

This allows us to put an upper limit on the electron density N_e of the regions responsible for the lines from the observed widths alone. The contribution to the line-width from Doppler broadening is given by

$$\Delta \nu_{LD} = 2 \sqrt{\ln 2} \frac{\nu}{c} \left[\frac{2kT_e}{m_H} + \frac{2}{3} \langle V_t^2 \rangle \right]^{1/2} \tag{8}$$

where $\langle V_t^2 \rangle^{1/2}$ is the rms turbulant velocity in the region, T_e is the electron temperature and m_H the mass of the emitter (hydrogen). The effective final width can be approximated by

$$\Delta \nu_L^2 = \Delta \nu_{LD}^2 + \Delta \nu_{LP}^2. \tag{9}$$

In Fig. 1 we have plotted the expected width of the H 272α recombination line as a function of electron density. The width has been calculated using Equations (7), (8) and (9) for two different temperatures and assuming an rms turbulent velocity of 20 km s^{-1} which is typical for Hɪɪ regions. As can be seen from this figure, the width increases sharply for $N_e > 50$ cm^{-3} irrespective of the temperature of the region. 85 per cent of
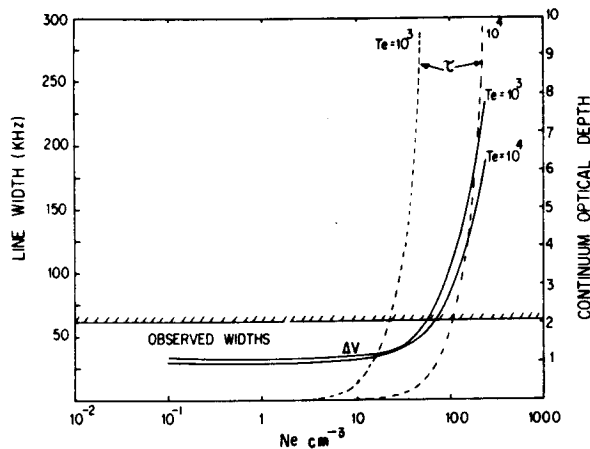

Figure 1. Expected width (FWHM) of the H 272α line (solid line) and continuum optical depth at 325 MHz (dashed line) as a function of electron density at two electron temperatures. Path length through the gas is assumed to be 50 pc. The hatched horizontal line indicates the maximum observed width from Paper I.

the lines observed in the survey reported in Paper I have widths < 60 kHz, which corresponds to an upper limit for the electron density of 60 cm^{-3}. Although the observed widths of the remaining 15 per cent of the lines are indicated as being > 60 kHz in Paper I, they may be made up of multiple components and therefore the actual widths of the individual components can be much smaller. Even so, the maximum width of the line, assuming it to be a single component, corresponds to an upper limit for the electron density of 100 cm^{-3}. In Fig. 1 we have also plotted the continuum optical depth at 325 MHz as a function of density assuming a path length of 50 pc. It is interesting that, if these regions have sizes of a few tens of parsecs along the line of sight, then their continuum optical depth at this frequency exceeds unity for densities > 50 cm^{-3}. As the region becomes optically thick the recombination lines merge with the continuum and become undetectable, at least under LTE conditions.

3. Analysis of lines observed toward blank regions and SNRs

Blank regions for our purposes were defined in Paper I as areas in the galactic plane where the continuum emission at 5 GHz is a minimum over the telescope beam of $2° \times 6$ arcmin used for these observations. The 5-GHz high-resolution map of Altenhoff *et al.* (1978) was used to select 6 such regions. There are no discrete continuum sources within these regions. Fig. 2 shows a typical blank region. The H 272α line has been detected towards all the six such directions.
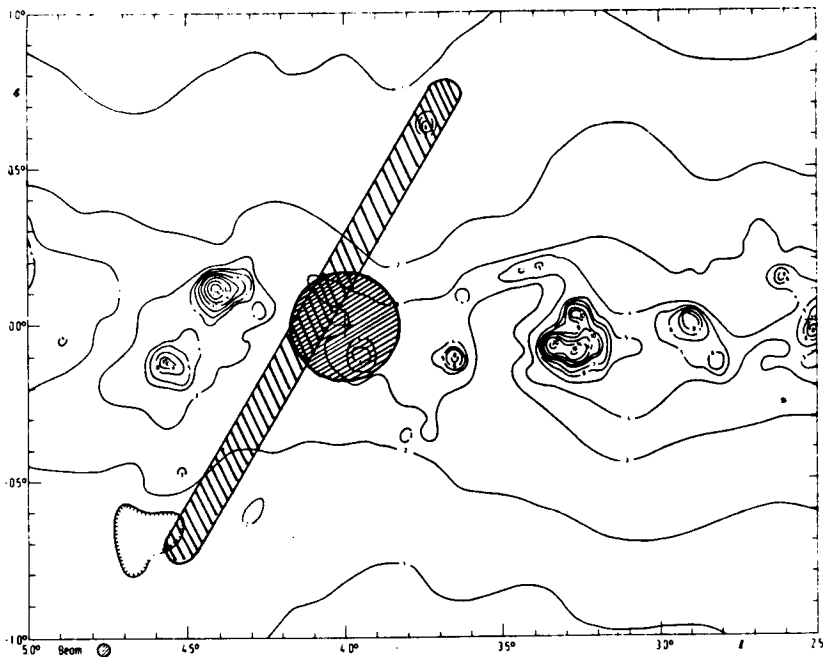

Figure 2. A typical blank region (see text) in the galactic plane for the beam used in the H 272α survey (elongated hatched area). The circular hatched area represents the beam used by Lockman (1976) who observed H 166α line at this position. The 5 GHz continuum map is from Altenhoff *et al.* (1978).

The line emission observed toward blank regions would fall under the category of galactic ridge recombination lines. Such lines were first detected near 18 cm (157α line) by Gottesman & Gordon (1970). Subsequently, similar lines have been reported towards selected positions by Gordon & Gottesman (1971), Jackson & Kerr (1971), Gordon & Cato (1972), Gordon, Brown & Gottesman (1972), Jackson & Kerr (1975) and Mebold et al. (1976). Lockman (1976) and Hart & Pedlar (1976b), in another approach, have observed the H 166α line emission (near 21 cm) at a number of positions along the galactic plane ($b = 0°$) separated by $0°.5$ to $1°$ in galactic longitude from $l = 0°$ to $l = 70°$. Some of these positions correspond to regions of continuum minimum as in the earlier studies.

In general, recombination lines are not expected from SNRs. Therefore the directions towards them are similar to the blank regions. The only difference is the presence of a strong background source in addition to the galactic nonthermal background.

In Paper I, H 272α line observations have been reported towards 11 directions corresponding to 10 well-known SNRs. Two of the adjacent directions observed (near W 44) corresponds to the same SNR. Recombination lines at higher frequencies have been detected earlier towards at least three of these SNRs (Cesarsky & Cesarsky 1973a, b; Bignell 1973; Downes & Wilson 1974; Pankonin 1975). Dulk & Slee (1972, 1975) have observed a turnover in the continuum spectrum of some of these sources at 80 MHz, which is attributed to free-free absorption by the line-of-sight ionized gas.

In this section we shall make use of the line parameters observed at 325 MHz (Paper I) and higher-frequency measurements to determine or put constraints on the parameters of the line-emitting region. Towards the blank regions and SNRs it is reasonable to assume that the lines observed at the two frequencies originate in the same gas (this may not be true in the direction of HII regions). We can only determine those parameters which have very different functional dependence on the observable quantities like line temperature T_L and width ΔV. Using Equations 1 to 5 and departure coefficients from Salem & Brocklehurst (1979), it can be shown that, for low electron densities, the intensity of recombination lines at a high frequency (e.g. H 166α) and of that at a low frequency (e.g. H 272α) has very different dependence on the electron density in the line-emitting region. This is a consequence of the dominance of the spontaneous emission at high frequencies and that of stimulated emission due to the background radiation at low frequencies. The line intensity due to spontaneous emission is proportional to the emission measure and therefore to the square of the electron density in the gas. On the other hand, if stimulated emission is dominant, the line intensity is essentially proportional to the electron density itself because of the similar dependence of the non-LTE factor $b_n\beta_n$ on the electron density.

3.1 A Model for Interpretation of the Observed Line Intensities

We shall adopt a simple plane-parallel homogeneous cloud model (Fig. 3) in which the electron temperature T_e and the electron density N_e are uniform. The cloud extends over a path length L along the line of sight, resulting in an emission measure $EM = N_e^2 L$. T_0 represents the radiation originating behind the cloud. The cloud cannot be assumed to fill the telescope beam of $2° \times 6$ arcmin used for the H 272α
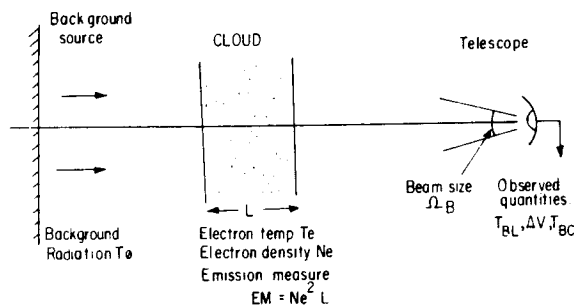
Figure 3. Schematic model used for interpretation of recombination lines in the direction of blank regions and SNRs.

observations. The H 157α and the H 166α emission in the blank regions extend over $b = \pm 0°.5$ perpendicular to the galactic plane (Gordon, Brown & Gottesman 1972; Lockman 1976; Hart & Pedlar 1976b). Assuming the gas to be present uniformly over this range we get a beam dilution factor of 0.6 for the H 272α observations. In all our analysis we have used this value for beam dilution, for the H 272α line.

In this model, the expected line brightness temperature is given by

$$T_{BL} = \frac{\Omega_C}{\Omega_B} T_L \tag{10}$$

where (Ω_C/Ω_B) is the beam dilution factor, and T_L is the line temperature calculated using Equation (1). For any specified value of N_e, T_e, EM and line width ΔV, the line and continuum optical depths τ_L and τ_C can be calculated using equations given in Section 2. b_n and β_n can be obtained using the computer code of Broklehurst & Salem (1977). Further, if T_0 and T_N are given, the expected T_L can be calculated using Equation (1).

3.2 *Electron Density of the Gas*

Based on the above model it turns out that the electron density is almost uniquely determined if we use the observed intensities of the H 166α and H 272α lines. From observations of Lockman (1976) the H 166α line measurements are available within 0°.3 in longitude for all the blank regions observed (Paper I) and for two of the positions the H 166α measurements are within the Ooty beam. The observed H 272α line parameters (Paper I), T_{BL}, ΔV and V_{LSR} and the measured total continuum temperature T_{BC} are given in Table 1 for all the blank regions. The peak H 166α line temperature observed by Lockman (1976) at the nearest position is also given in this table. We assume that the two observations pertain to the same gas.

The corresponding parameters for eight of the SNR directions are given in Table 2. The parameters of the high-frequency lines observed towards two of these directions (W 49B and W 44) and the references are also given in Table 2. The source 3 C 391, towards which the H 272α line is narrower than the high-frequency lines will be discussed elsewhere. For the other 6 directions we use the H 166α line parameters

K. R. Anantharamaiah

Table 1. Observed parameters for blank regions.

Source	H 272α Parameters				H 166α[1]		5 GHz continuum Temp.[2] K
	Line Temp. K	Width km s^{-1}	Velocity V_{LSR} km s^{-1}	T_{BC} K	T_L K	T_C K	
G 2.1−0.0	0.81 (0.13)	47 (4)	5 (2)	740	< 0.016	13.3 (1.2)	0.56
G 4.2−0.0	1.28 (0.24)	33 (5)	7 (2)	690	0.045 (15)	10.0 (0.5)	0.40
G 9.4+0.1	0.61 (0.13)	42 (7)	10 (3)	730	0.054 (14)	12.1 (0.7)	0.40
G 15.7−0.0	0.86 (0.14)	58 (5)	43 (2)	610	0.051 (15)	08.9 (1.0)	0.36
G 17.6−0.3	0.67 (0.11)	47 (4)	30 (2)	630	0.027 (14)	08.1 (1.2)	0.34
G 21.2−0.0	0.64 (0.11)	26 (3)	98 (2)	580	0.038 (15)	10.4 (0.7)	0.34
	0.46 (0.08)	54 (6)	25 (3)				

1. From Lockman (1976)
2. Estimated from the maps of Altenhoff et al. (1978)

Table 2. Observed parameters towards SNRs.

	H 272α line parameters						High frequency parameters						
Source	V_{LSR} km s^{-1}	T_L K	ΔV km s^{-1}	T_{BC} K	T_{BSNR} K	T_0 K	Line	V_{LSR} km s^{-1}	T_L K	ΔV km s^{-1}	T_C K	Ref.	τ_{80}
1	2	3	4	5	6	7	8	9	10	11	12	13	14
G 357.7 −0.1 ····	−7.9(1.3)	1.3(2)	40(3)	930	276	534	166α		0.027(18)		13.4(1.4)	1	0.12(25)
G 6.6 −0.1 W 28	11(2)	1.1(2)	43(4)	900	284	592	166α		0.052(19)		16.7(1.2)	1	···
G 11.2 −0.3 ···	37(2)	0.8(2)	23(6)	760	189	475	166α		0.06		15.4	2	0.09(38)
G 21.8 −0.6 ···	54(2)	0.7(12)	44(5)	790	151	470	166α		0.038(14)		7.7(6)	1	···
G 23.0 −0.3 ···	68(2)	0.84(14)	55(4)	770	136	453	166α		0.058(14)		13.2(1)	1	···
G 34.6 −0.6 W 44	48(1)	0.87(16)	21(3)	830	325	576	166α	50	0.036(09)		30	3	···
G 39.2 −0.3 3C396	84(2)	0.66(13)	21(5)	570	141	356	166α		0.017(12)	21	6.4(0.6)	4	0.02(09)
G 43.2 −0.1 W 49	63(1)	1.2(2)	35(3)	690	315	503	134α / 166α	65(10) / 60	0.019(03) / 0.02	45 / 30	19 / ···	5	0.44(09)

1. Lockman (1976) 2. Hart & Pedlar (1976) 3. Bignell (1973) 4. Cesarsky & Cesarsky (1973b) 5. Downes & Wilson (1974)

observed by Lockman (1976) or Hart & Pedlar (1976b) at the nearest position. These parameters are also listed in the table. For four of these six positions the available H 166α measurement are within the Ooty beam and for the other two positions they are within $0°.4$ of the beam centre. The measured value of 80 MHz optical depth, wherever available, is also given in Table 2.

Using Equation (1) and the model described above, it is possible to find those combinations of N_e, T_e and EM which produce the observed intensities of both the H 166α and the H 272α lines. The procedure adopted was as follows. For a set of specified N_e and T_e, in the range 0.1–100 cm^{-3} and 100–10000 K respectively, the emission measure required to produce the observed intensity of the H 272α line was calculated using Equations (10) and (1). For the blank regions the background temperature T_0 in Equation (1) was taken to be $T_{BC}/2$ (Table 1). For the SNR directions T_0 was estimated as follows. We first estimated the expected average brightness temperature T_{BSNR} over the $2° \times 6$ arcmin beam, due to the SNR, using the 408 MHz flux density, spectral index and size given in the catalogue of Clark & Caswell (1976). The contribution to the observed brightness temperature T_{BC} (given in Table 2) from the galactic nonthermal background was then taken to be

$$T_{Bg} = T_{BC} - T_{BSNR}.$$

The effective temperature of the radiation coming from behind the cloud for each of the directions was calculated using

$$T_0 = T_{BSNR} + T_{Bg}/2$$

where it is assumed that half of the observed background originates behind the cloud. The values of T_0 are given in Table 2. As the path lengths involved are not very large, we used $T_N = 0$. A dilution factor $(\Omega_C/\Omega_B) = 0.6$ was used in all the calculations.

Similar calculations were performed to obtain the required emission measure to produce the observed high-frequency line intensity. In these calculations, we used a beam dilution factor of unity. For the blank regions we used $T_0 = T_C/2$ and $T_N = 0$. For the SNR directions all of the observed continuum at high frequencies was assumed to originate behind the cloud. The respective widths of the lines at two frequencies, wherever available, was used for the calculation. Otherwise, the observed H 272α line width was used for both low- and high-frequency lines.

The results of these calculations are shown in Fig. 4 for the blank region G 4.2 − 0.0 and for the SNR G 357.7 − 0.1. In these figures we have plotted the required emission measure as a function of electron density N_e to produce the observed intensity of the H 272α and H 166α lines, for four different electron temperatures. The intersection point of the 272α and 166α curves at each of the temperatures gives the electron density N_e (and the corresponding EM) which will explain both the observed H 166α and H 272α line intensities. It is remarkable that irrespective of the temperature T_e and emission measure EM of the region there is only a very small range of electron densities (bounded by the two vertical dashed lines) that is consistent with the line intensities at both frequencies. This range is less than a factor of 1.5 and for temperatures above 1000 K the required density has practically a unique value.

Using the adopted model, the accuracy of the electron density as determined above depends only on the accuracy of the measurements of the line parameters and the estimate of the beam dilution factor. Based on the errors of the line intensities the derived density is determined to within a factor of two. If the beam dilution changes by
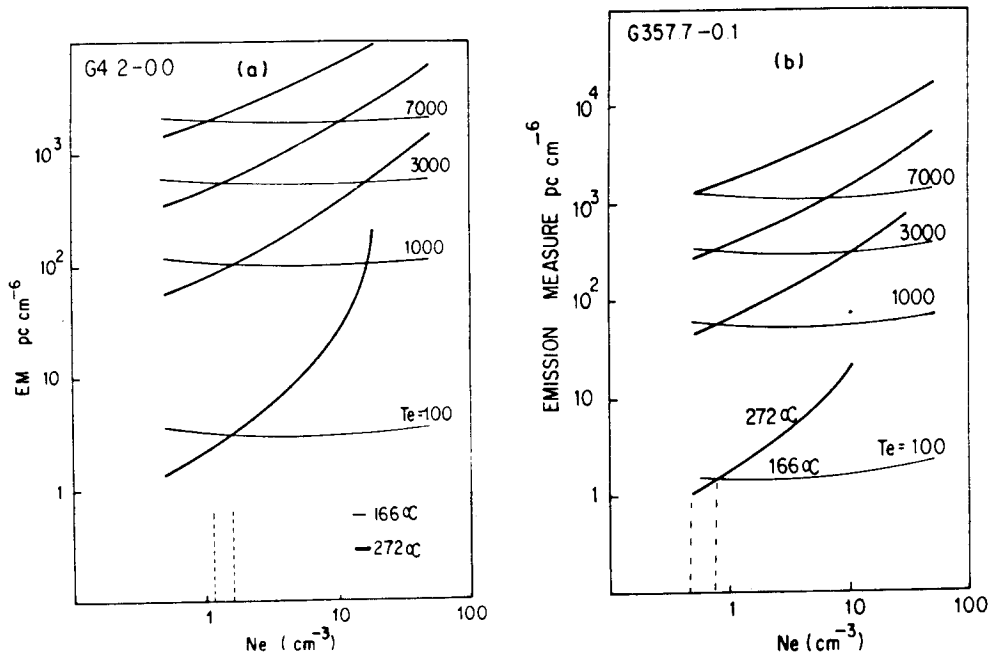
Figure 4. The relation between emission measure and electron density of the gas in order to produce the observed intensity of the H 166α (thin lines) and H 272α (thick lines) lines towards (a) the blank region G 4.2 − 0.0, and (b) for the SNR direction G 357.7 − 0.1. The calculation (see text) is done for different electron temperatures indicated. The intersection point of the thick and thin lines gives the density of the gas. The vertical dashed lines indicate the range of densities allowed for the temperature range of 100 to 7000 K.

a certain factor then the derived density changes by a similar factor. An increase in the beam dilution (*i.e.* smaller angular-size for the cloud) for the H 272α line results in a decrease in density. An increase in T_0 will increase the derived density.

In the case of W 49, for which two high-frequency measurements are available, we obtained the density in a similar way using both the high-frequency lines. The densities which are derived differ only by a factor of 1.5.

The densities derived from similar calculations for all the blank regions and SNRs are given in column 2 of Tables 3 and 4 respectively. They are in the range of 0.5–7 cm^{-3}. We regard these densities as reliable to within a factor of two. It should be noted here that these densities are the true (or local) electron densities of the line-emitting regions and not the rms electron density as in the case when it is derived (for strong HII regions) from continuum measurements. In the latter case, as also in the case of high-frequency recombination lines, the emission is proportional to the square of the electron density. But at low frequencies, due to the strong dependence of b_n and particularly β_n on the electron density, the strength of the line emission is proportional to the density itself. Therefore, if there is any clumping in the gas, then the clumps themselves should have this derived density and the size of the region should increase to make up for the decreased filling factor. In other words, if the emission measure of this gas is fixed, say by other considerations, then the size of the region (along the line of sight) can be $\geqslant EM/N_e^2$ depending on the filling factor of the ionized gas at density N_e.

Table 3. Derived parameters for blank regions.

Source	N_e cm^{-3}	Upper limits from T_C (5 GHz)			Upper limits from PSR DM			Lower limits with $L > 50$ pc	
		EM cm^{-6} pc	T_e K	L pc	L pc	EM cm^{-6} pc	T_e K	EM cm^{-6} pc	T_e K
G 2.1 − 0.0	0.5	4000	11000	16000	800	200	2100	12.5	500
G 4.2 − 0.0	1.2	3600	10000	3600	400	400	2500	50	800
G 9.4 + 0.1	6.0	3500	8000	97	60	2160	6000	1800	5000
G15.7 − 0.0	2.5	2800	5000	448	160	1000	3100	312	1300
G17.6 − 0.3	2.0	2500	7000	625	200	800	4000	200	1600
G21.2 − 0.0	4.0	2500	8500	156	100	1600	6000	800	4000

Table 4. Properties of ionized gas towards SNRs

Source	N_e cm^{-3}	Upper limit from PSR DM			Lower limit with $L > 50$ pc		Values for $T_e = 5000$		
		L pc	T_e K	EM cm^{-6} pc	T_e K	EM cm^{-6} pc	EM cm^{-6} pc	L pc	τ_{80}
G 357.7 − 0.1	0.7	570	2500	280	700	25	700	1430	0.11
G 6.6 − 0.1	2.5	160	4000	1000	2000	312	1300	208	0.21
G 11.2 − 0.3	4	100	7000	1600	4500	800	850	53	0.14
G 21.8 − 0.6	3.8	105	6000	1500	4000	722	1050	73	0.17
G 23.0 − 0.2	4	100	5000	1600	3000	800	2000	125	0.33
G 31.9 + 0.0	7	51	8000	2500	7000	2450	1200	25	0.20
G 34.6 − 0.6	1.1	363	6000	440	1800	61	360	297	0.06
G 39.2 − 0.3	0.7	570	5000	280	1500	25	300	612	0.05
G 43.2 − 0.1	1.5	266	3000	600	1100	113	1000	44	0.16

3.3 *Electron Temperature and Emission Measure*

Since in the model we are considering there are only three parameters N_e, T_e and *EM* which characterize the ionized region, and we have used two measured quantities (the intensity of the H 166α and H 272α lines) to determine N_e, the other two parameters are related to each other through the observed intensity of the H 166α or the H 272α line. The method used for determining the electron density N_e ensures that the relation between T_e and *EM* will be very similar irrespective of whether we use the H 166α or the H 272α line intensity to relate them. A determination of, or putting a constraint on, either T_e or *EM* (or even the path length L) will decide or impose a constraint on the other quantity.

Fig. 5 shows the relation between *EM* and T_e. The lines marked 272α and 166α in these figures represent *EM* as a function of T_e required by the intensities of these lines given the electron density N_e which was obtained in the previous section. As expected, the two curves are very similar. On the right-hand ordinate is also marked the effective path length obtained simply from the relation $L = EM/N_e^2$.
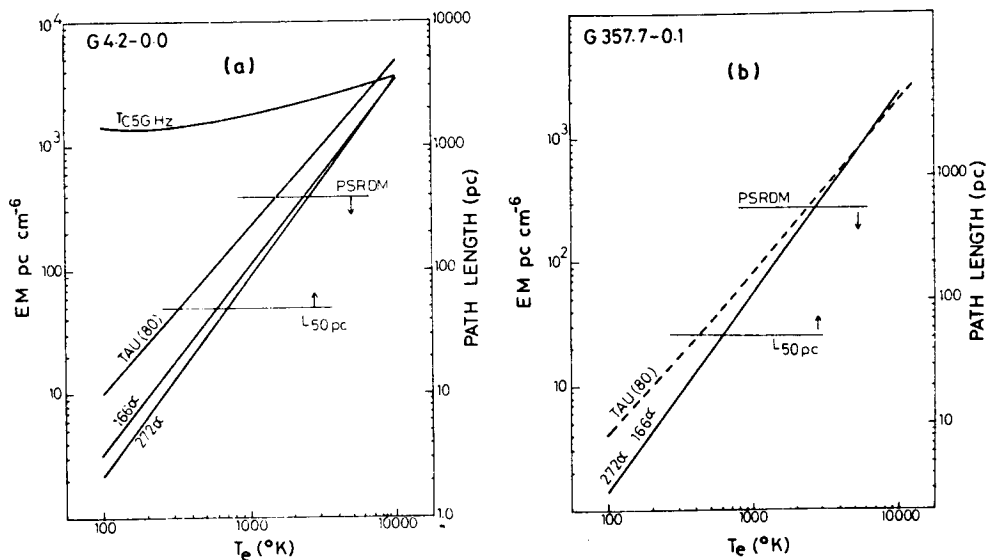
Figure 5. Constraint on the emission measure, electron temperature and path length through the gas towards (a) the blank region G 4.2 − 0.0 and (b) the SNR direction G 357.7 − 0.1, from considerations of average interstellar electron density (line marked PSR DM), 5 GHz continuum emission (TC5GHz) and geometry of the line emitting region (L 50 pc). See text for arguments. The lines marked 166α and 272α represent the constraint based on the observed recombination lines. An electron density derived from Fig. 4 is used (see Table 2). The combination of T_e and EM required to produce an 80 MHz continuum optical depth of 0.25 (Tau 80) is also shown. In the case of G 357.7 − 0.1 no constraint can be imposed using 5 GHz continuum.

Unfortunately, there is no other measured quantity available which can be directly attributed to this gas and which depends on T_e, EM or L in a different way, to impose a constraint on any of these parameters. However, we can put some limits on these parameters from three considerations.

The first of these is based on the thermal continuum emission from this gas. At a sufficiently high frequency like 5 GHz, the contribution to the galactic background from the nonthermal radiation is very small particularly in the blank areas. Therefore most of the observed continuum at 5 GHz will be thermal. We have estimated the average continuum temperature at 5 GHz at each of the observed blank regions using the high-resolution maps of Altenhoff *et al.* (1978). The values are given in Table 1. We now require that the ionized gas which produces the recombination lines should not produce more than this observed continuum. This will impose an upper limit on the EM of the gas which in turn will imply an upper limit on the electron temperature. The nearly horizontal line marked TC5GHz in Fig. 5 represents this constraint. The emission measure cannot be above this line. Combining this limit with the relation between EM and T_e we can get an upper limit for T_e. The upper limits for all the blank regions are given in Table 2. The upper limits for EM are in the range of 2500–4000 cm^{-6} pc and for T_e in the range of 5000–10000 K. We cannot use this argument for the SNR directions since most of observed 5 GHz continuum is emitted by the SNR itself.

Given the density of the gas an upper limit on its path length can be imposed using the pulsar dispersion measure. Vivekanand & Narayan (1982) have analysed the dispersion measure toward 224 pulsars and obtained a model for the galactic electron density of the form

$$N_e(z) = 0.030 + 0.020 \ \exp\left(\frac{-|z|}{70}\right) \mathrm{cm}^{-3} \tag{11}$$

where z (pc) is the height above the galactic plane. The first term in this expression represents a distributed medium of average density $\langle N_e \rangle = 0.03 \ \mathrm{cm}^{-3}$ having a scale height in excess of 300 pc. The second term describes the contribution from localized higher-density ionized regions (e.g. HII regions) which occur in the galactic plane with a scale height of 70 pc. The regions responsible for the recombination lines observed towards blank regions and SNRs can be considered to fall in this category. We can use the second term of Equation (11) together with N_e determined above, to set an upper limit to the effective path length through the gas responsible for the recombination lines.

If N_e is the density of a region lying along a line of sight and L_{gal} is the path length through the entire Galaxy, then the above result imposes a restriction on the effective path length L through the region of the form

$$N_e \frac{L}{L_{gal}} \leqslant 0.02 \ \mathrm{cm}^{-3}$$

or

$$L \leqslant \frac{0.02}{N_e} L_{gal}.$$

Using the N_e determined for the blank regions and SNRs and taking $L_{gal} = 20$ kpc we obtain upper limits of 60–400 pc for the effective path length through the gas responsible for the observed lines. The horizontal lines marked PSRDM in Fig. 5 represents this upper limit. The upper limit on L implies an upper limit on EM which in turn implies an upper limit on T_e. These upper limits are given in Tables 3 and 4. In most of the cases these upper limits are lower than those implied by the 5 GHz continuum. The upper limits implied by the pulsar dispersion measure are not as rigorous as the upper limits from the continuum. This is because the contribution to the interstellar electron density from HII regions derived by Vivekanand & Narayan (1982) is an average over the entire Galaxy; in addition, in their analysis there was a scarcity of pulsars in the longitude range of interest here.

It is possible to set a lower limit to the electron temperature and therefore to the emission measure from geometrical considerations. In Fig. 5 it can be seen that a lower electron temperature implies a lower emission measure which in turn implies a smaller effective path length, since the density of the region is fixed. For a temperature of 100 K, (which is typical for HI clouds) the required path lengths are in the range of 0.2–2 pc.

As pointed out by Shaver (1976), with such small path lengths the geometry of these regions would be very peculiar. The scale height of this gas is estimated to be 70–80 pc from a study of the latitude extent of the H 166α emission by Lockman (1976) and Hart & Pedlar (1976b). Therefore this gas would have dimensions of ~ 100 pc in the direction perpendicular to the line of sight. For low electron temperatures, the above small effective path lengths would require these regions to be in the form of thin

extensive sheets or small cloudlets distributed along the line of sight with a very small filling factor. Both these geometries would be inconsistent with the smooth observed line profiles of width 30–50 km s^{-1}.

It is difficult to set any rigorous lower limit to the temperature from these geometrical considerations. However it is reasonable to expect that the path length be comparable to or larger than the lateral extent of the gas, which is of the order of 50–100 pc. This lower limit on the path length requires that the electron temperature be higher than a few thousand degrees. The lower limits to the temperature and *EM* based on a path length of 50 pc through the gas are given in Tables 3 and 4.

It may be possible to set a lower limit to the electron temperature of the ionized region only based on the electron density. This is because ionization always results in heating of the gas. In fact the main source of heating in most of the interstellar regions is through ionization after which the excess energy carried by the liberated electron is converted into kinetic energy of the particles through collisions (Spitzer 1978). The electron density of 1–7 cm^{-3} derived above for the blank regions and SNRs imply high ionization rates for hydrogen. It may not be possible to achieve such electron densities without heating the gas to a considerable degree. We recall that an average of 0.5 eV excess energy of the ionizing photons, over the 13.6 eV ionization potential would result in a kinetic energy of the electrons corresponding to a temperature of > 3000 K.

We conclude that the temperature of the gas responsible for the lines observed towards blank regions and SNRs is greater than a few thousand degrees.

Although there is another measured quantity (τ at 80 MHz) pertaining to the ionized gas, along the line of sight to some of the SNRs (Dulk & Slee 1975), it cannot be used to put an independent constraint on any of the parameters. If one requires that the gas produce all of the observed τ_{80}, the relation between *EM* and T_e is very similar to the corresponding relation for explaining the observed intensity of the H 272α and H 166α lines. In Fig. 5(b) the line marked TAU (80) represents this relation for the observed value of τ_{80} towards the source G 357.7 − 0.1. As can be seen, this line runs almost parallel to the lines marked 272α and 166α and therefore does not give a new constraint. However, we can require that the gas responsible for the recombination lines should not produce more than the observed 80 MHz optical depth. This is easily satisfied for all the SNR directions we have considered. The 80 MHz optical depth of the recombination line emitting regions calculated with $T_e = 5000$ K are given in Table 4. It turns out that the line-emitting regions can account for most of the observed 80 MHz optical depth.

4. Lines observed towards Hɪɪ regions

4.1 *General Considerations*

These are possibly the best-studied ionized regions of the Galaxy. They appear as prominent sources in the radio continuum surveys of the galactic plane (*e.g.* Altenhoff *et al.* 1970, 1978; Haynes *et al.* 1978) and are more numerous than any other type of galactic radio source.

There are 30 such 'conventional' Hɪɪ regions towards which the H 272α line has been detected in the observations reported in Paper I. The observed line intensity and width for 21 of these directions are given in Table 5. The intensity of low-frequency recombination lines from these Hɪɪ regions is expected to be very weak due to the effect

Table 5. Optical depth and sizes of HII regions and upper limits on density.

Source	T_{BL} (272α) K	ΔV km s^{-1}	$N_{e,max}$ cm^{-3}	$N_{e,HII}$ cm^{-3}	T_c K	EM cm^{-6} pc	τ_{325}	size θ arcmin	Beam dilution
1	2	3	4	5	6	7	8	9	10
G 2.3+0.2	0.48(12)	18(5)	20		3700	4.2 E+04	0.6	3.6	0.005
G 4.4+0.2	0.39(09)	66(13)	90		5700	6.7 E+04	6.5	4.2	0.006
G 6.0−1.2 M8	1.10(20)	43(4)	50	370	7700	3.4 E+05	2.0	4.5	0.006
G 7.0−0.3 M20	0.63(13)	30(6)	30	143	7500	7.7 E+04	0.4	5.7	0.008
G 8.1+0.2	0.64(12)	47(7)	60		6500	4.7 E+05	3.0	2.9	0.004
G 10.2−0.3 W31	0.77(13)	51(4)	65	356	5700	1.0 E+06	7.0	3.1	0.004
G 12.8−0.2 W33	0.72(13)	32(4)	35	1774	7900	4.8 E+06	23.0	0.8	0.001
G 14.0−0.1	1.00(20)	38(3)	45		5800	8.4 E+04	0.6	3.3	0.005
G 15.1−0.7 M17	0.67(12)	41(5)	50	581	9100	1.8 E+06	7.0	9.1	0.076
G 16.9+0.7 M16	0.73(11)	53(3)	70		6100	6.9 E+04	0.5	8.1	0.067
G 20.7−0.1	0.45(11)	19(6)	15	96	5900	7.4 E+04	0.5	4.5	0.006
G 24.8+0.1 W42	1.00(15)	77(4)	100	51	5800	2.8 E+04	0.2	5.0	0.007
G 25.4−0.2 3C385	0.49(10)	77(15)	100	224	7100	2.9 E+05	2.0	3.2	0.004
	0.27(10)	26(11)	30						
G 27.3+0.2	0.98(16)	85(6)	120		7400	8.6 E+04	0.4	2.9	0.004
G 28.8+3.5 W40	0.27(05)	35(4)	40	273	8500	1.2 E+05	0.5	5.8	0.008
	0.36(06)	44(4)	55						
G 29.9+0.0	1.00(20)	35(4)	40	> 111	6100	1.7 E+05	1.0	4.3	0.006
G 30.8+0.0 W43	1.20(20)	41(3)	50	205	6000	5.2 E+05	4.0	5.5	0.008
G 35.1−1.6 W48	0.61(11)	55(6)	70	> 20	7250	1.5 E+04	0.08	5.3	0.007
G 37.8−0.2 W47	0.31(09)	33(11)	35	> 130	8400	5.8 E+04	0.3	2.9	0.004
	0.76(09)	49(7)	60						
	0.68(09)	17(3)	5						
G 49.0−0.3 W51B	0.86(11)	23(4)	10	87	9000	1.2 E+05	0.5	7.0	0.058
G 206.0−2.1 W16	0.40(20)	28(5)	20	18	6000	8.6 E+03	0.06	55	0.46

Parameters for the HII regions are taken from the high-frequency measurements of Shaver & Goss (1970b), Silverglate & Terzian (1979), Viner, Vallée & Hughes (1979), and Downes et al. (1980)

of pressure broadening and beam dilution. Most of these HII regions have been studied elsewhere using both the continuum and high-frequency recombination lines. The electron density, temperature and emission measure obtained from such studies, if they are available, are given in columns 5, 6 and 7 of Table 5. The upper limit on the electron density of the gas responsible for the H 272α lines obtained from their observed widths are given in column 4. From a comparison of columns 4 and 5 of this table, it is clear that, with the exception of one or two sources, the HII regions themselves cannot be responsible for the observed H 272α lines. Column 8 of the table shows that most of these HII regions are optically thick at 325 MHz and for this reason too they are unlikely to produce the observed recombination lines. Further, for most of these sources the beam dilution factor is 10^{-2}–10^{-3} (column 10) due to the 2° × 6 arcmin antenna beam used in these observations which is much larger than the few arcmin sizes of these sources (column 9). The beam dilution will reduce the intensity of the already weakened lines (due to pressure broadening and optical depth) to practically undetectable levels. Therefore, the observed H 272α lines in these directions *must* arise in some gas other than the HII regions.

We first compare the location of this gas with respect to the HII regions, as implied by the observed velocities. In column 3 of Table 6 we have given the observed velocity of the H 272α line and in column 4, that of a high-frequency line. There is generally a very good agreement between the two velocities, particularly if we take into account the errors in their determination (they are 2–5 km s^{-1} for both). In any case there is always a substantial emission of the H 272α line at the velocity of the high frequency line. This immediately implies that the lower-density gas responsible for the H 272α line is associated with the HII region. The most reasonable picture for this association is that the low-density gas forms the outer envelope of the dense HII region responsible for the observed high-frequency lines and the continuum.

The picture that emerges therefore is that the HII regions which are prominent in the continuum (having densities of $10^2 - 10^4$ cm^{-3}), and which produce most of the observed high-frequency recombination lines, have low-density envelopes which can give rise to low-frequency recombination lines. The high-density cores make practically no contribution to the low frequency lines. There is observational support for the above picture. In a classic paper, Brocklehurst & Seaton (1972) showed that in order to explain the observed line-to-continuum ratio as a function of frequency it is necessary to use models of HII regions which contain extensive outer regions of low density. Hart & Pedlar (1976a) have observed H 166α line emission from 13 positions near the HII region W 3 and conclude that there is an extended low-density region associated with this object.

Based on such a model, we shall now derive or put constraints on the parameters of the low density envelopes from the observed intensity of the H 272α line.

4.2 *Electron Temperature of the Low-Density Envelopes*

The temperature of the low-density envelopes of HII regions is unlikely to be very different from that of the cores. The temperature of a fully ionized region is basically governed by the abundance of heavy elements like oxygen, nitrogen, neon *etc.* (Osterbrock 1974). The electron temperature depends only weakly on the effective temperature of the exciting star or stars and the density of the gas. Since the core and the

outer envelope were presumably parts of the same cloud, the abundance of heavy elements in them is unlikely to be very different. If the exciting star for the outer envelope is embedded in the core, then a case can be made for the outer envelope to be at a somewhat higher temperature. This is because there will be a hardening of the radiation emerging after ionization of the core, which will on the average impart a slightly higher kinetic energy to the electrons liberated in the outer regions. On the other hand, the lower density in the outer regions can slightly reduce the collisional de-excitation of the coolant ions (Oii, Oiii *etc.*) thereby increasing the efficiency of the cooling process. The actual temperature will therefore depend on the relative importance of these two processes. If the exciting star is in the outer region itself, then only the second argument applies and the resulting temperature can be somewhat lower than that of the core.

For our purposes, it is reasonable to assume that the electron temperature of the low-density envelope is essentially the same as that of the core. These temperatures for each of the Hii regions is given in column 6 of Table 5. Most of these temperatures are derived from the H 110α measurements by Downes *et al.* (1980), on the assumption of LTE.

4.3 *Electron Density and Emission Measure*

We have used an isothermal, uniform density model (Fig. 6) similar to the one used for the case of blank regions and SNR directions. The difference here is that the high-density core of the Hii region is embedded inside the low-density region responsible for the H 272α line. This can have two effects. The continuum radiation from the core can cause stimulated emission of the recombination line in the lower-density gas in front of it. Secondly, if the core is optically thick at this frequency, then it can block the line emission originating from behind it. However, the angular sizes of these Hii regions (5 arcmin) are very small compared to the $2° \times 6$ arcmin beam used for observations, and therefore their contribution to the continuum temperature is, in most cases, negligible compared to the nonthermal galactic background which is nearly uniform over the beam. We can therefore neglect to first order both the above effects.

The expected H 272α line brightness temperature is given by Equations (10) and (1). For nearby Hii regions, the background temperature T_0 was taken to be equal to the
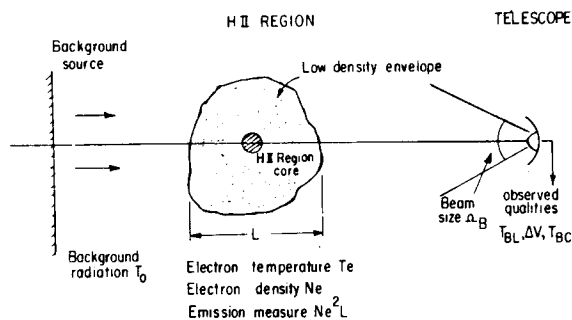

Figure 6. Schematic of the model for interpreting recombination lines observed towards Hii regions. High-frequency recombination lines arise mainly from the central core which is also prominent in the radio continuum. The low-frequency line originates in the outer envelope.

observed continuum brightness temperature T_{BC} listed in Table 6. For those HII regions which are known to be at the far kinematic distance, T_0 was calculated using

$$T_0 = (T_{BC} - T_{HII})/2 + T_{HII}$$

where T_{HII} is the beam-averaged brightness temperature of the HII region core calculated using its T_e, N_e, EM and its angular size θ derived from high frequency measurements (see Table 5). In the case of the HII region W 16 (the Rosette nebula) we have used $T_0 = 0$ since it is in the anticentre direction. In addition this source is known to be of low density (10–15 cm^{-3}) and large angular size ($\sim 1°$). Therefore the observed H 272α line can originate from the HII region itself. We have used $T_N = 0$ for all the cases.

We have calculated the emission measure for densities in the range 0.1–100 cm^{-3} necessary to produce the observed intensity of the H 272α recombination line towards each of the 19 HII regions. We have used the electron temperatures derived from high-frequency measurements (Table 5). The calculations were carried out using beam dilution factors of 0.3 and 0.6. The above calculations were not carried out for 11 of the

Table 6. Velocity, background temperature and derived parameters of HII regions.

						Derived parameters		
Source	T_{BC} K	V_{LSR} H 272α km s^{-1}	V_{LSR} H 110α km s^{-1}	Distance kpc	T_0 K	N_e cm^{-3}	EM cm^6 pc	L pc
1	2	3	4	5	6	7	8	9
G 2.3 + 0.2	750	9 (2)	5	...	375	...	....	...
G 4.4 + 0.2	700	4 (5)	5.7	17.0	350	1.8	1100	356
G 6.0 − 1.2	660	−4 (1)	3.0	1.4	660	15	7000	29
G 7.0 − 0.3	720	6 (2)	14	1.5	720	7.5	1700	31
G 8.1 + 0.2	770	25 (3)	22	...	770	...	....	...
G 10.2 − 0.3	610	15 (2)	13	9.0	300	3.6	2800	188
G 12.8 − 0.2	730	26 (2)	30	4.4	730	4	1500	92
G 14.0 − 0.1	680	24 (2)	31.5	4	680	4	1600	84
G 15.1 − 0.7	810	9 (2)	11.5	2.4	810	8	3000	50
G 16.9 + 0.7	610	20 (1)	28	2.2	610	7.5	2600	46
G 20.7 − 0.1	590	47 (3)	57	13.8	300	1.1	380	290
G 24.8 + 0.1	660	83 (2)	107	9	330	4	3500	186
G 25.4 − 0.2	650	54 (6) 107 (5)	59	13.2	340	2	1100	276
G 27.3 + 0.2	640	93 (2)	33	15.2	320	4	4800	318
G 28.8 + 3.5	450	72 (2) 19 (2)	0.7	0.7	450	15	3500	15
G 29.9 + 0.0	650	91 (2)	98.5	9	330	3.5	2500	189
G 30.8 + 0.0	830	95 (1)	90	7.1	830	3	1500	149
G 35.1 − 1.6	460	34 (3)	43	3.2	460	7	3500	67
G 37.8 − 0.2	480	0.3 (5) 44 (3) 87 (1)	61	11.5	250	4.8	5500	241
G 49.0 − 0.3	690	61 (2)	60.5	6.6	690	3.1	1400	138
G 206.0 − 2.1	100	5 (2)	7(3)	1.4	0	11	4000	29

Distances are taken from Downes *et al.* (1980) or Radhakrishnan *et al.* (1972)

30 H$_{II}$ regions (towards which H 272α line was detected) either because the velocity did not match that of the high-frequency line, or the distance to the H$_{II}$ region was unknown.

The results of these calculations are shown for two of the H$_{II}$ regions (M 20, M 16) in Fig. 7. The two curves marked 272 (0.3) and 272 (0.6) in the figure shows the required emission measure, as a function of electron density, to produce the observed H 272α line intensity, if the beam dilution factor is 0.3 and 0.6, respectively.

It is reasonable to assume that the extent of the envelope along the line of sight is comparable to its linear size in the perpendicular direction, obtained using a source size of 0°.6 to 1°.2 (*i.e.* a dilution factor of 0.3 to 0.6 in east-west) and known distances. We thus impose the restriction that the emission measure and electron density of the gas be related by

$$EM = N_e^2 L_\perp$$

where $L_\perp$ is the size of the line-emitting region perpendicular to the line of sight given by

$$L_\perp = dD\theta_\alpha$$

where d is the distance to the H$_{II}$ region, θ_α is the east-west beam of the telescope, and D is the beam dilution factor. The region is assumed to fill the beam in the north-south direction (*i.e.*, the angular extent of the gas is > 6 arcmin).

The two inclined straight lines marked L (0.3) and L (0.6) in Fig. 7 shows the above restriction on the density and emission measure of the region for beam dilution factors 0.3 and 0.6 respectively. The intersection of these lines with the corresponding curves marked 272 (0.3) and 272 (0.6) define the emission measure and electron density of the envelope from which the H 272α line is observed. As can be seen from Fig. 7, the derived electron density N_e increases with decreasing beam dilution factor D. The upper limit on N_e obtained from the width of the H 272α line implies a lower limit of 0.2 for the beam dilution factor.

The electron density, emission measure and the path length through the gas obtained assuming the most probable beam dilution factor of 0.6, are given in Table 6. If the
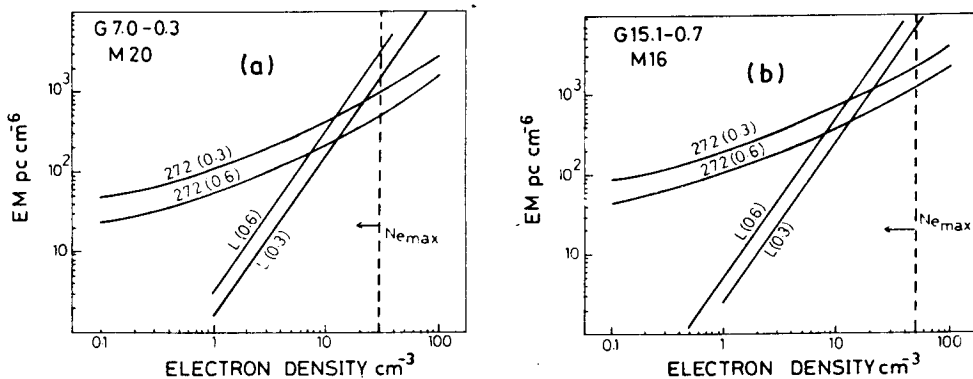

Figure 7. Constraints on the emission measure and electron density of the low-density envelopes of H$_{II}$ regions (a) M 20 and (b) M 16, based on the observed intensity of H 272α lines and geometrical considerations (see text). The vertical dashed line is the upper limit on the electron density implied by the width of the line.

dilution factor D is greater than 0.6 by some factor, then the derived densities will be lower by nearly the same factor. The densities are in the range $1-10 \, \text{cm}^{-3}$, emission measures are in the range $1000-4000 \, \text{pc cm}^{-6}$ and the corresponding path lengths through the regions are 30–300 pc. The temperatures of these are assumed to be the same as those of the cores which are in the range 5000–9000 K.

5. Discussion of the derived parameters

5.1 *Blank Regions and SNRs*

An examination of Tables 2 and 4 reveals that the parameters characterizing the ionized gas towards SNRs and blank areas in the galactic plane are quite similar. The regions responsible for the observed lines have densities in the range of $1-6 \, \text{cm}^{-3}$, their temperatures are greater than a few thousand degrees but less than about 8000 K, and they have emission measures of 500 to 3000 $\text{cm}^{-6} \, \text{pc}$. The corresponding path lengths through the gas are in the range 50–200 pc. The similarity is not surprising since the gas which is observed in these directions (SNRs and blank regions) is the same as that responsible for galactic ridge recombination lines observed at centimetre wavelengths. Any phenomenon that is as widespread and uniform as the galactic ridge recombination lines must have some very general explanation.

The parameters derived here account for the observed strength of the galactic ridge recombination lines, and the high-frequency recombination lines towards SNRs. This is necessarily true since we have made use of these lines to constrain the parameters. They account for most of the 80 MHz continuum optical depth observed by Dulk & Slee (1975). The gas can possibly also account for the background thermal emission seen in the galactic plane.

The parameters characterizing the gas responsible for the galactic ridge recombination lines and the lines towards supernova remnants have been a topic of discussion in the literature since the first observations by Gottesman & Gordon (1970). Shaver (1976) has made the most comprehensive study of the available data on these lines. Combining this data with the few low-frequency (408 and 386 MHz) recombination line measurements then available (Pankonin *et al.* 1974; Pankonin 1975; Gordon *et al.* 1974) he has concluded that the lines arise in HII regions having electron densities $5-10 \, \text{cm}^{-3}$, diameters of 20–200 pc and emission measures of $2000-4000 \, \text{cm}^{-6} \, \text{pc}$. He favours temperatures of the order of 5000 K. Lockman (1980) has analysed the H 166α data near $l = 36°$ and concludes that the gas responsible for the line emission has a temperature of 1000 K, an emission measure of a few hundred cm^{-6} pc and a density of $1 \, \text{cm}^{-3}$.

The parameters derived by us for the line-emitting gas in the direction of SNRs and blank regions are consistent with an interpretation in terms of high-temperature, moderate-density $(1-10 \, \text{cm}^{-3})$ regions. Our results are very similar to those of Shaver (1976) who also used low-frequency recombination lines for deriving the parameters. In fact the technique adopted by us is similar in many ways to that of Shaver (1976). Although we cannot quantitatively estimate the temperature of the gas, we also favour higher temperatures (a few thousand degrees) based on considerations of pulsar dispersion measure and geometry of the line-emitting region.

Based on these results alone it is not possible to decide the origin of this gas. With the small path lengths of 50–200 pc derived for these regions, they can not be regarded as some component of the general interstellar medium; the average path length through the Galaxy at these longitudes is $\sim$ 20 kpc. This gas could be in the form of a number of small low-density HII regions, low density envelopes of bright HII regions seen in the galactic plane or some other kind of ionized gas produced in localized regions of the interstellar medium. This question will be addressed to in a subsequent paper.

5.2 *H II Regions*

The density and emission measure derived by us for the gas responsible for the observed H 272α recombination lines towards HII regions are about a factor of 10–100 (in most cases more likely 100) less than that of conventional HII regions. There are only a very few low-frequency recombination line observations towards HII regions available in the literature to compare with our results (*e.g.*, Gordon *et al.* 1974; Pankonin *et al.* 1974; Parrish *et al.* 1977; Pedlar *et al.* 1978).

Parrish *et al.* (1977), based on 300 MHz observations towards W 51B, find that this line arises in a region of density $<$ 30 cm^{-3} and has an angular size 25 arcmin. They also argue that this low-density gas is associated with the discrete source W 51B, due to the observed similar velocities of high and low-frequency lines. This is in fact the argument we have used as a starting point for deriving the parameters. Pedlar *et al.* (1978) interpret their low-frequency observations towards the galactic centre in terms of low-density gas with $N_e \sim$ 10 cm^{-3}. They note that any single component model requires that the electron density be $\sim$ 10 cm^{-3} (irrespective of EM and T_e) to account for the low-frequency lines towards the galactic centre. The parameters derived by us are quite consistent with these results.

There is at least one HII region (W 16, the Rosette nebula) in our survey (Paper I) which is known to be large and of low density for which we can directly compare the parameters derived by us with those from high-frequency measurements. We obtain a density of 11 cm^{-3} and EM of 4000 pc cm^{-6} which are consistent with the parameters ($N_e =$ 9 cm^{-3}, $EM =$ 2600 pc cm^{-6}) derived by Pedlar & Matthews (1973) using the H 166α line, and by Viner, Vallée & Hughes (1979) ($N_e =$ 16 cm^{-3}) using the H 100α recombination line.

A comparison of the parameters for the low-density envelopes of conventional HII regions derived here and those for the regions responsible for the lines observed towards blank regions and SNRs reveals that they are very similar. As the lines observed towards SNRs and blank regions are attributed to the gas responsible for the galactic ridge recombination lines, the above similarity immediately suggests that the latter may also arise in low-density extended envelopes of HII regions seen in the galactic plane. This suggestion will be pursued further in a subsequent paper (Anantharamaiah 1985b) where it will in fact be shown that most of the galactic ridge recombination lines do arise in the extended envelopes of conventional HII regions prominent in the radio continuum surveys. HII regions are so numerous in the inner part of the Galaxy that given the kind of low-density envelopes suggested by the analysis in this paper, they intersect practically every line of sight in the galactic ridge having $l \leqslant 40°$, thereby giving rise to recombination lines in every direction within this range.

Acknowledgements

References

Altenhoff, W. J., Downes, D., Goad, L., Maxwell, A., Rinehart, R. 1970, *Astr. Astrophys. Suppl.*, **1**, 319.
Altenhoff, W. J., Downes, D., Pauls, T., Schraml, J. 1978, *Astr. Astrophys. Suppl.*, **35**, 23.
Anantharamaiah, K. R. 1985a, *J. Astrophys. Astr.*, **6**, 177, (Paper 1).
Anantharamaiah, K. R. 1985b, In preparation.
Bignell, R. C. 1973, *Astrophys. J.*, **186**, 889.
Brocklehurst, M., Leeman, S. 1971, *Astrophys. Lett.*, **9**, 35.
Brocklehurst, M., Salem, M. 1977, *Computer Phys. Commun.*, **13**, 39.
Brocklehurst, M., Seaton, M. J. 1972, *Mon. Not. R. astr. Soc.*, **157**, 179.
Brown, R. L., Lockman, F. J., Knapp, G. R. 1978, *A. Rev. Astr. Astrophys.*, **16**, 445.
Cesarsky, D. A., Cesarsky, C. J. 1973a, *Astrophys. J.*, **183**, L143.
Cesarsky, D. A., Cesarsky, C. J. 1973b, *Astrophys. J.*, **184**, 83.
Clark, D. H., Caswell, J. L. 1976, *Mon. Not. R. astr. Soc.*, **174**, 267.
Downes, D., Wilson, T. L. 1974, *Astr. Astrophys.*, **34**, 133.
Downes, D., Wilson, T. L., Bieging, J., Wink, J. 1980, *Astr. Astrophys. Suppl.*, **40**, 379.
Dulk, G. A., Slee, O. B. 1972, *Aust. J. Phys.*, **25**, 429.
Dulk, G. A., Slee, O. B. 1975, *Astrophys. J.*, **199**, 61.
Gordon, K. J., Gordon, C. P., Lockman, F. J. 1974, *Astrophys. J.*, **192**, 337.
Gordon, M. A., Brown, R. L., Gottesman, S. T. 1972, *Astrophys. J.*, **178**, 119.
Gordon, M. A., Cato, T. 1972, *Astrophys. J.*, **176**, 587.
Gordon, M. A., Gottesman, S. T. 1971, *Astrophys. J.*, **168**, 361.
Gottesman, S. T., Gordon, M. A. 1970, *Astrophys. J.*, **162**, L93.
Griem, H. R. 1967, *Astrophys. J.*, **148**, 547.
Hart, L., Pedlar, A. 1976a, *Mon. Not. R. astr. Soc.*, **176**, 135.
Hart, L., Pedlar, A. 1976b, *Mon. Not. R. astr. Soc.*, **176**, 547.
Haynes, R. F., Caswell, J. L., Simons, L. W. J. 1978, *Aust. J. Phys. Astrophys. Suppl.*, **45**, 1.
Jackson, P. D., Kerr, F. J. 1971, *Astrophys. J.*, **168**, 29.
Jackson, P. D., Kerr, F. J. 1975, *Astrophys. J.*, **196**, 723.
Lockman, F. J. 1976, *Astrophys. J.*, **209**, 42.
Lockman, F. J. 1980, in *Radio Recombination Lines*, Ed. P. A. Shaver, D. Reidel, Dordrecht, p. 185.
Mebold, U., Altenhoff, W. J., Churchwell, E., Walmsley, C. M. 1976, *Astr. Astrophys.*, **53**, 175.
Oster, L. 1961, *Rev. Mod. Phys.*, **33**, 525.
Osterbrock, D. E. 1974, *Astrophysics of Gaseous Nebulae*, Freeman, San Francisco.
Pankonin, V. 1975, *Astr. Astrophys.*, **38**, 445.
Pankonin, V., Parrish, A., Terzian, Y. 1974, *Astr. Astrophys.*, **37**, 411.
Parrish, A., Conklin, E. K., Pankonin, V. 1977, *Astr. Astrophys.*, **58**, 319.
Pedlar, A., Davies, R. D. 1980, in *Radio Recombination Lines*, Ed. P. A. Shaver, D. Reidel, Dordrecht, p. 171.
Pedlar, A., Davies, R. D., Hart, L., Shaver, P. A. 1978, *Mon. Not. R. astr. Soc.*, **182**, 473.
Pedlar, A., Matthews, H. E. 1973, *Mon. Not. R. astr. Soc.*, **165**, 381.
Radhakrishnan, V., Goss, W. M., Murray, J. D., Brooks, J. W. 1972, *Astrophys. J. Suppl. Ser.*, **24**, 49.
Salem, M., Brocklehurst, M. 1979, *Astrophys. J. Suppl.*, **39**, 633.
Shaver, P. A. 1975, *Pramana*, **5**, 1.

Shaver, P. A. 1976, *Astr. Astrophys.*, **49**, 1.

Shaver, P. A., Goss, W. M. 1970, *Aust. J. Phys. Astrophys. Suppl.*, **14**, 133.

Silvergate, P. R., Terzian, Y. 1979, *Astrophys. J. Supp.*, **39**, 157.

Spitzer, L. 1978, *Physical processes in the Interstellar Medium*, Wiley-Interscience, New York.

Viner, M. R., Vallée, J. P., Hughes, V. A. 1979, *Astr. J.*, **84**, 1335.

Vivekanand, M., Narayan, R. 1982, *J. Astrophys. Astr.*, **3**, 399.

Wilson, T. L. 1980, in *Radio Recombination Lines*, Ed. P. A. Shaver, D. Reidel, Dordrecht, p. 205.